TECHBRIEF

Alkali-Silica Reaction Mechanisms and Detection: An Advanced Understanding

Publication No. FHWA-HRT-14-079

FHWA Contacts: Paul Virmani, HRDI-60, (202) 493-3052, paul.virmani@dot.gov; Fred Faridazar, HRDI-20, (202) 493-3076, fred.faridazar@dot.gov.

This document is a technical summary of the Federal Highway Administration project that is fully documented in a separate, forthcoming technical report under the same title, *Alkali-Silica Reaction Mechanisms and Detection: An Advanced Understanding* (FHWA-HRT-14-078).

Introduction

The deterioration caused by alkali-silica reaction (ASR) was first described 70 years ago in the pioneering paper by Stanton and has since been extensively researched.[1] The traditional attempts to mitigate ASR in concrete structures focused on preventing and/or reducing the amount of gel formed by modifying the chemical environment. Limiting the alkali content of concrete, using supplementary cementitious materials, or using chemical admixtures all have been found to be effective and have been extensively used for that purpose. However, the complexity of chemical and mechanical mechanisms of ASR made it difficult to develop reliable quality control test methods and performance prediction models. Therefore, increased understanding of the fundamental mechanisms of ASR may lead to the development of additional (and possibly better) options for ASR control and for reactivity characterization of susceptible aggregates.

The main purpose of this research was to investigate the fundamental mechanisms involved in the ASR process and to advance approaches to detect the damage caused by ASR. A more indepth understanding of the mechanisms underlying ASR, combined with the methods to detect ASR damage developed in the course of this study, is expected to help establish more reliable methods of mitigating ASR and increasing the design life of newly constructed concrete structures.

U.S. Department of Transportation
Federal Highway Administration

Research, Development, and Technology
Turner-Fairbank Highway Research Center
6300 Georgetown Pike
McLean, VA 22101-2296

www.fhwa.dot.gov/research

Fundamental Mechanisms

Experiments and Modeling of Chemical Sequence of ASR Processes

To advance the understanding of the fundamental mechanisms of ASR and more comprehensively evaluate the rate of chemical reactions, a series of model reactant experiments were conducted using selected silica minerals (α-cristobalite and chalcedony). This TechBrief presents the results obtained from testing of α-cristobalite. This mineral was selected to represent the siliceous component of the ASR-prone aggregate because it is known for its reactivity. In addition, it only contains negligible amounts of nonevaporable water and thus easily facilitates quantification of the amount of silica dissolved during the model reactant experiments. During testing, the cristobalite was exposed to an aqueous mixture of calcium hydroxide ($Ca(OH)_2$) and three different types of alkali hydroxide solutions (0.7 M of potassium hydroxide (KOH), 0.7 M of sodium hydroxide (NaOH), and 0.35 M of KOH + 0.35 M of NaOH) roughly representing the pore solution of reactive concrete. Each test was conducted at three different temperatures (38, 55, and 80 °C). The quantitative data generated during these experiments—including the degree of chemical changes in the composition of solution, the mass changes of $Ca(OH)_2$, and the mass changes of reactive silica minerals—allowed for establishment of the sequence of chemical steps involved in ASR.

Specifically, this study identified a distinct sequence of chemical steps associated with the ASR process. These steps are marked as I to IV in figure 1: (I) the formation of calcium silica hydrate (C-S-H), (II) the formation of high alkali and low calcium silica hydrate (C-(Na/K)-S-H), (III) the increase in concentration of silica ions in the solution, and (IV) the formation of ASR gels ((Na/K)-S-H). Based on this sequence, it appears that the overall ASR process starts with the dissolution of silica, which, once in solution, rapidly reacts with the available Ca^{2+} ions to produce C-S-H. During this period (step I in figure 1), the concentrations of alkali ions and the values of pH remain more or less constant, but the amounts of remaining reactive silica and the $Ca(OH)_2$ significantly decrease.

Once the $Ca(OH)_2$ in the reacting system is exhausted, the process of removing dissolved silica from the solution also ceases (or significantly decreases), leading to an increase in the concentration of Si^{4+} ions. These dissolved Si^{4+} ions can further react with previously formed C-S-H, generating polymerized (amorphous) C-(Na/K)-S-H with a reduced (compared with typical C-S-H gel) value of Ca/Si molar ratio (step II in figure 1). After the formation of this amorphous and polymerized C-(Na/K)-S-H gel, the rate of change in the concentration of alkalis decreases, but the concentration of Si^{4+} ions keeps increasing up to a certain (maximum) point (step III in figure 1). Following this action, a decrease in the concentrations of Si^{4+} and alkali ions can be observed. It is believed that the point when the concentrations of the Si^{4+} ions and alkali ions start to decrease coincides with onset of ASR (step IV in figure 1).

Figure 1. Sequence of steps in the ASR process obtained from the reacting system (mixture of α-cristobalite, $CA(OH)_2$, and KOH solution at 55 °C).

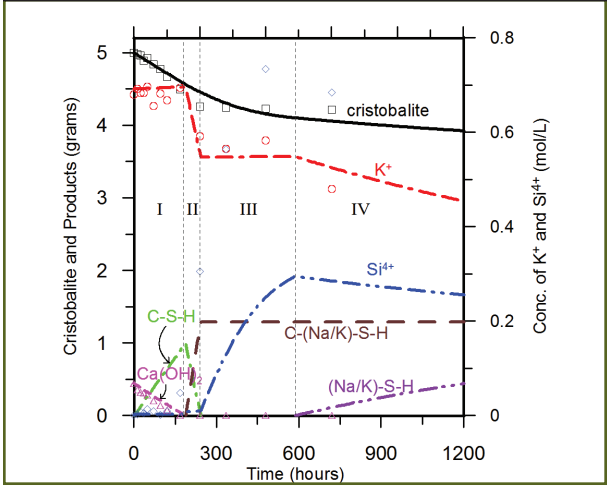

Lines represent modeling results, whereas individual points represent experimental data.
□ = cristobalite.
Δ = $Ca(OH)_2$.
o = concentration of K^+ ions.
◊ = concentration of Si^{4+} ions.

The results of this model reactant experiments were used to develop a thermodynamic model for the ASR process. The model accounts for such parameters as chemical equilibrium between $Ca(OH)_2$, reactive silica (α-cristobatlie), alkali ions, other various secondary species, and solid products. When developing the thermodynamic model, it was assumed that the ASR process simulated in the model reactant method is the surface-controlled (rather than transport-controlled) reaction between the solution and the exposed surface of reactive silica. The model considers formation of three major products: C-S-H, C-(Na/K)-S-H, and (Na/K)-S-H.

The results produced by this model are shown as lines in figure 1. The proposed model produced results that are in good agreement with the experimental results (represented by the points). In addition, this model can reproduce the distinct features of experimental results, such as the consumption of cristobalite and $Ca(OH)_2$, changes in the concentration of alkali ions, the timing of the increase in silica ions concentration, and the change in pH values. This model also confirms the existence of, and offers indication of possible mechanism for, the threshold value of alkali concentration in concrete. By using the experimental results to provide the thermodynamic properties of reactive silica minerals, this model can be used to evaluate the kinetics of ASR, including the evolution of changes in concentrations of various species in the pore solution and the formation of reaction products.

Role of Aggregates

To better understand the role of aggregate in the basic mechanism of ASR, a variety of aggregate sources were examined. The selected aggregates represented a range of reactivity, mineralogy,

Table 1. Master table of aggregate sources and their properties.

Source		Aggregate		Potentially Reactive Mineralogy	Percent Expansion[1]		
Location	Source Name	Size	Rock Type		ASTM C1293	MCPT 56-day	ASTM C1260
Ontario, Canada	ON1	CA	Limestone (Q)	Siliceous inclusions	0.181	0.149	0.35
North Carolina	NC1	CA	Argillite (Q)	Microcrystalline quartz	0.192	0.149	0.53
South Dakota	SD1	CA	Quartzite (Q)	Chert, strained quartz	0.109	0.095	0.22
Massachusetts	MA3	CA	Lithic greywacke (Q)	Matrix with high silica igneous minerals	N/A	0.096	0.41
New Mexico	NM1	CA	Igneous gravel	Glassy volcanic	0.251	0.185	0.90
El Paso, TX	TX1	FA	Volcanic sand	Glassy volcanic	0.59	0.44	0.64
Illinois	IL3	FA	Glacial sand	Chert, weathered chert	N/A	0.121	0.41
Nebraska 1	NE2	FA and CA	Glacial gravel and sand	Chert	0.09	0.091	0.23
Nebraska 2	NE4	FA and CA	Glacial gravel and sand	Chert and jasper	0.15	0.115	0.46
Pittsburgh, PA	PA3	FA	Glacial sand	Chert	N/A	0.111	0.25

[1]The percent expansion results were obtained via personal communication with Dr. Prasada Rangaraju and were generated during work completed by Clemson University.
ASTM = American Society for Testing and Materials; MCPT = miniature concrete prism test.
CA = coarse aggregate; FA = fine aggregate.
N/A = not applicable; Q = quarried aggregate.

and rock types from a wide geographic distribution (see table 1). The reactive mineralogy and other pertinent components of each source were identified. These same aggregate sources were then examined in the reacted state in a concrete system, and the ASR induced changes were identified.

The amount and type of reactive silica identified in each source varied but in general included microcrystalline quartz, strained quartz, chert, cristobalite, and various silica-rich volcanic rocks, including rhyolite, andesite, and dacite. The miniature concrete prism test (MCPT) specimens made from each source identified in table 1 exhibited deleterious expansion (based on a 0.04-percent expansion limit after 56 days of testing). Besides expansion, other evidence of reaction included spalling of the concrete surface; gel deposits; reaction rims around aggregate particles; cracks through, around, and radiating out from the aggregates; altered paste at the interfacial transition zone, and chemical alterations of the aggregate. All MCPT concrete specimens showed some evidence of ASR, but not all prisms showed all aforementioned features. The only variable in the concrete systems examined was the aggregate, suggesting that not only is the aggregate's role to supply reactive silica, but that its other characteristics also influence how the concrete behaves and how it exhibits evidence of ASR reaction.

Influence of ASR on the Chemistry of Pore Solution

The kinetics of changes in the chemistry of the solution in systems undergoing ASR can provide useful information regarding the extent of ASR over time and may offer some indication of potential expansion. In this research, the chemistry of pore solutions obtained from mortars prepared with both reactive aggregate (TX1 sand) and the nonreactive aggregate (Ottawa sand) were examined. Because of the space limitation, this report only presents the results of mortars prepared with reactive aggregate and cured in a moist environment at three different temperatures (23, 38, and 55 °C). The threshold alkali concentration for the ASR process was obtained from the mortar samples exposed at 55 °C, and this value (0.22 mol/L) was used to investigate the kinetic laws that best explain the observed changes in alkali concentration in the pore solution undergoing ASR.

The nature of the linear plot shown in figure 2 indicates that the alkali ion concentrations in pore solution can best be expressed as the first order reaction, as shown in figure 3.

$[Na^+ + K^+ - 0.22]_t$ is the concentration of available alkali ions present in the solution of the system undergoing ASR ($mol \cdot L^{-1}$) at a certain time (t), and k_{exp} is the experimental rate constant (s^{-1}). The values of k_{exp} at three different test temperatures were determined from the slope of the linear regression line shown in figure 2. Figure 4 shows that the experimental data is fairly well represented by the proposed rate equation (figure 3). This kinetic analysis, which has R^2 values over 0.905, strongly suggests that the proposed rate equation (the first order reaction) for the changes in concentration of alkali ions as a function of time provided very reasonable predictions of the actual concentrations. Because reduction of the alkali concentration was not observed in the control mortars made with nonreactive aggregate, the reduction of alkali concentration in pore solution was the direct result of ASR. Therefore, these results also indicate that the rate of ASR in cementitious systems can be correlated (via the first order reaction) with the concentration of the alkali ions in the pore solution.

Influence of Lithium Ions in ASR Systems

The use of lithium-based chemical admixtures for the purposes of ASR mitigation has been extensively studied for more than 60 years. These studies resulted in several proposed mechanisms by which Li^+ ions may potentially control ASR. However, none of these

Figure 2. The plots of ln[Na^+ + Na^+ - 0.22] versus time for reactive mortar (TX1 sand) with a water-to-cement ratio (w/c) of 0.55 (R0.55) mixtures reacting at different temperatures (23, 38, and 55 °C).

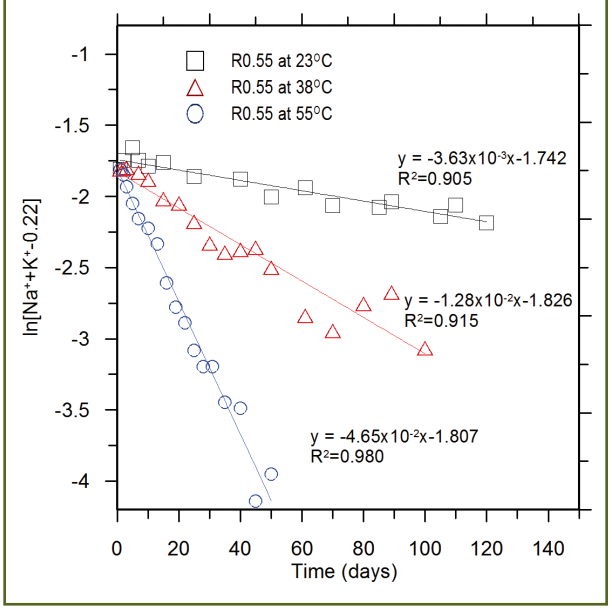

Figure 3. First order reaction for changes in alkali concentra

$$-\frac{d[Na^+ + K^+ - 0.22]_t}{dt} = k_{exp}[Na^+ + K^+ - 0.22]_t$$

Figure 4. Change in alkali concentration [Na^+ + K^+] over time.

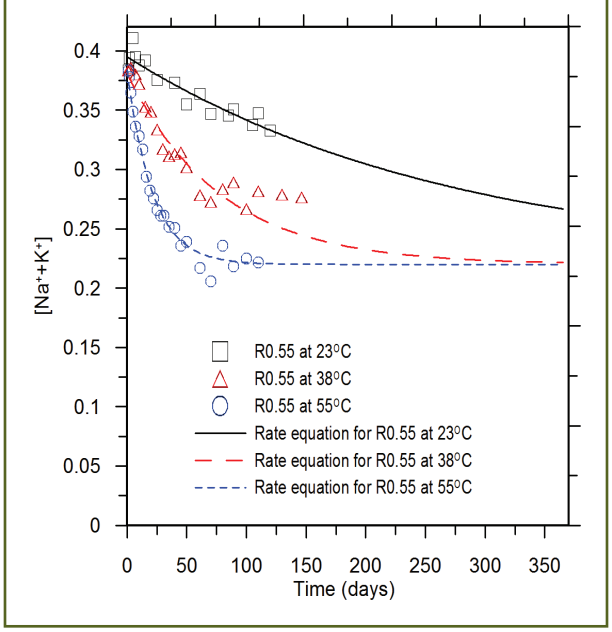

mechanisms fully explains the role of lithium in controlling ASR. In this context, several experiments were conducted during this study in an effort to understand the role of lithium ions in ASR systems.

Loss of Li^+ Ions From Pore Solution During Early Hydration Period

Pore solutions obtained from numerous mixtures (cement slurries and mortars) were analyzed to develop better understanding of the interaction between lithium ions and other ions present in the pore solution.

The cement slurry experiments were designed to investigate the effect of timing of the addition of lithium nitrate ($LiNO_3$) on the concentration of lithium ions in pore solution during the early hydration period. It has been shown that at early age the loss of Li^+ ions from pore solution is the result of their incorporation in the developing hydration products and not the results of sorption by the existing hydrates. In addition, pore solutions obtained from various mixtures of mortar samples (containing nonreactive aggregate) were analyzed to quantify the effects of water-to-cement ratio, $LiNO_3$ dosage, and length of curing time on the loss of lithium ions during the early stages of hydration. The results indicated that about half (50~60 percent) of the originally added Li^+ ions will be removed from the pore solution after about two days of hydration, regardless of the initial amount of admixture added. Furthermore, the percentage of Li^+ lost remained constant in mixtures prepared at the same w/c. However, that percentage will decrease with the increase in the w/c value.

Modeling of the Loss of Li^+ Ions From Pore Solution

The data generated during the experiments presented in the previous section were examined thoroughly to develop a model to predict the extent of Li^+ ion loss from the pore solution. Based on this model, the rate of loss of Li^+ ions per kilogram of cement can be represented by the equation shown in figure 5.

Figure 5. Rate loss of Li^+ ions per gram of cement.

$$r(t) = \frac{k[\mathrm{Li}]_0 \alpha_u \beta \tau^\beta}{t^{\beta+1} \cdot \left[1 - \frac{0.24\alpha_u}{\mathrm{w/c}} \exp\left[-\left(\frac{\tau}{t}\right)^\beta\right]\right]^{\frac{k-0.24}{0.24}} \cdot \exp\left(\frac{\tau}{t}\right)^\beta}$$

Where:

t is the time since the start of hydration (hours).

k is the rate constant (unitless).

r(t) is the rate of loss of Li^+ ions per kilogram of cement ($mol \cdot kg^{-1} \cdot hr^{-1}$).

$[Li]_0$ is the initial concentration of Li^+ ions in the mix water ($mol \cdot kg^{-1}$).

α_u is the ultimate degree of hydration.

τ is the hydration time parameter (representing the time delay from mixing until setting).

β is the hydration shape parameter (representing the slope of the S-shaped curve of the degree of hydration).

It should be noted that all variables needed in figure 5 (except for the rate constant *k*) can be determined from the initial mix design of the cementitious system and properties of cement. The value of the rate constant (*k*) was determined during the model calibration process. The resulting value of *k* was 0.499. That value of *k* was, in turn, used as an input into the equation shown in figure 5.

Figure 6 shows the scatter plot of the experimentally determined versus predicted adjusted concentrations of lithium ions in the pore solution. This plot contains experimental data obtained from both, the mixtures used in the current study (mortars containing nonreactive aggregate) and literature.[2,3] Collectively, these data represent systems with five different cements, four different w/c (0.42, 0.47, 0.49 and 0.55), and 15 different $[Li]_0$ values (corresponding to eight different ratios of [Li]/[Na+K]). Individual points are located quite close to the equity line (R^2 = 0.98), indicating that the proposed model accurately predicts the experimental results.

This model can also predict the beneficial effect of the delayed release of $LiNO_3$ in paste or mortar systems. The concept of delayed release of $LiNO_3$ into the cementitious system might be explored further to develop a new lithium-ion delivery method that can minimize the early-age losses of the $LiNO_3$ admixture. In conclusion, the presented model appears to provide a useful tool for investigating the effects of various factors on the Li^+ ions concentration without the need for time-consuming experiments.

Study of the Role of Lithium Ions in Controlling ASR

This part of the study focused on the investigation of the effect of Li^+ ions on the chemical reactions involved in the ASR process. The experimental results show that the addition of the Li^+ ions to the reactive system prevents the very

Figure 6. Scatter plot of adjusted versus predicted adjusted concentrations (based on figure 5) of Li^+ ions in various pore solutions.

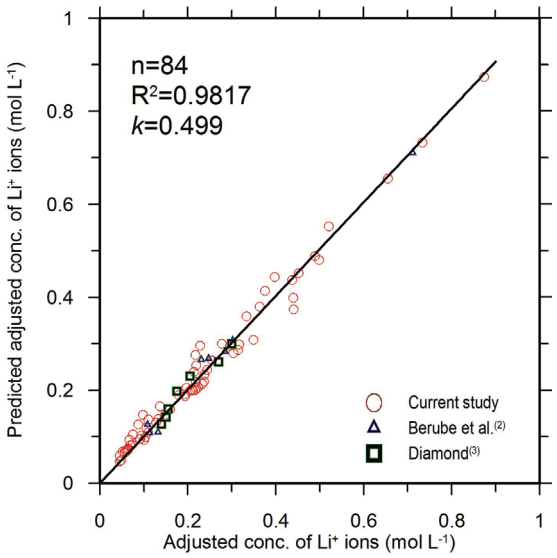

Note: o represents data from mortar samples with nonreactive aggregate, while Δ and □ represent data from pastes.

first step of the ASR process (i.e., the dissolution of silica) and thus hinders the subsequent steps.

Results from the model reactor experiments provided evidence for the mechanism by which the Li^+ ions can prevent the dissolution of silica during the early reaction period. This mechanism can be summarized as follows. The ASR process starts with the hydroxyl ions (OH^-) attacking the siloxane groups on the surface of reactive silica and breaking them down to form silanol groups. In turn, these silanol groups rapidly react with Li^+ and Ca^{2+} ions present in the pore solution and form reaction products composed of silica, calcium, and lithium. These reaction products serve as the physical barrier that surrounds the surface of the reactive aggregate and prevents further attacks of reactive silica by hydroxyl ions.

The study of the effects of Li^+ ions on the chemistry of the pore solution obtained from actual cementitious systems (mortar made with reactive aggregates) confirmed the results obtained from the model reactor experiment. The presence of Li^+ ions in the pore solution resulted in significant reduction of the amount of alkali ions being removed. On the other hand, the concentrations of Li^+ ions in the pore solution of mortars made with reactive aggregates also significantly decreased with time. This reduction in concentration of Li^+ ions might be the result of the formation of the Si-Li reaction products on the surface of the reactive aggregate. These products appear to prevent further attack of silica by hydroxyl ions. As a result, the rate of consumption of K^+ and Na^+ ions by ASR was significantly reduced (or even completely halted), thus leading to establishment of the more or less constant levels of alkali ions in the pore solution with time.

Role of Deicers on ASR

Deicers play a significant role in further intensifying existing distress mechanisms (including ASR already active in concrete), especially if concrete was not produced using quality materials and sound construction practices. The effects of deicers on paste and mortars with or without reactive aggregate were explored using expansion tests and microscopic analysis.

Mortar Bar Expansion Tests (Modified American Society for Testing and Materials (ASTM) C1260)

The ASTM C1260 standard mortar bar test was modified by replacing the 1 N NaOH solution with various deicers. The concentrations of these deicers were as follows: potassium acetate (KAc)—50 weight percent; NaCl—23 weight percent; magnesium chloride ($MgCl_2$)—25 weight percent; and calcium chloride ($CaCl_2$)—28 weight percent. The expansion data collected in the course of this study clearly demonstrate that mortars incorporating reactive aggregates undergo significantly higher expansion in the presence of KAc and NaCl deicers when compared with those containing nonreactive aggregates. The $MgCl_2$ and $CaCl_2$ deicers do not seem to contribute to ASR gel formation, and the observed expansions should therefore be attributed to the changes in the cement matrix itself.

Scanning Electron Microscopy With Energy Dispersive X-ray Spectroscopy (SEM-EDX) Investigation of Spratt, Jobe, and Ottawa Mortar Bars Exposed to KAc Deicer

The SEM-EDX examinations were performed on specimens prepared from mortar bars subjected to a modified ASTM C1260 test procedure in which the standard soak solution, 1 N NaOH, was replaced with various deicers. In addition, the test was performed at temperatures different than the standard ASTM C1260 temperature of 80 °C (e.g., 38 or 23 °C). These investigations confirmed that when incorporated in the cement matrix, the reactive aggregates do undergo active deterioration by ASR in the presence of the KAc deicer, as shown in figure 7. Deposits of a calcium-bearing potassium sulfate phase (secondary reaction product) were observed in cracks around the aggregate particles, along cracks in the matrix, and in some voids.

Figure 7. SEM-EDX micrograph of Spratt mortar with extensive cracking within aggregate and through matrix.

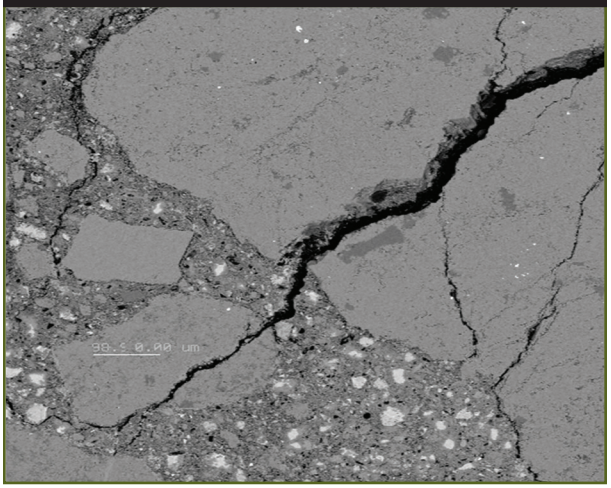

SEM-EDX Investigation of Concrete Exposed to NaCl, $MgCl_2$, and $CaCl_2$ Deicers Under Wetting and Drying (W/D) and Freezing and Thawing (F/T) Conditions

The interactions of concrete specimens containing nonreactive aggregate with three different deicers were investigated by exposing them to solutions of NaCl (23 weight percent), $MgCl_2$ (25 weight percent), and $CaCl_2$ (28 weight percent). To evaluate the influence of deicers on ASR under conditions resembling field exposure, a series of experiments were performed in which concrete specimens were exposed to deicers while being subjected to either wetting (at 4 °C) and drying (at 23 °C) or freezing (at -20 °C) and thawing (at 23 °C) cycles.

Deposits of $MgCl_2$ and brucite ($Mg(OH)_2$) were found in both matrix and air voids close to the edges of specimens exposed to $MgCl_2$ deicer under both W/D and F/T conditions (figure 8). Hexagonal plates of portlandite were observed in the air voids under W/D conditions, and cracks could be easily found in the specimen exposed to $CaCl_2$ deicer under F/T conditions. Friedel's salt ($Ca_2Al(OH)_6(Cl, OH) \cdot 2\ H_2O$) was observed close to the edges of specimens exposed to NaCl, $MgCl_2$, and $CaCl_2$ deicers under both W/D and F/T conditions, indicating the reaction of penetrating chlorides with the components of the matrix.

Figure 8. Deposit of $MgCl_2$ and $Mg(OH)_2$ in concrete exposed to $MgCl_2$ deicer after 275 W/D cycles.

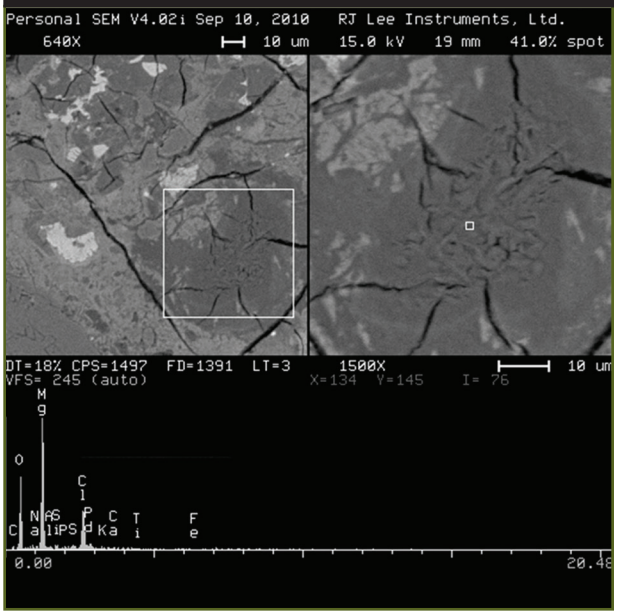

Advanced Approaches to Detect the Damange Caused By ASR

Two approaches (passive acoustic emission monitoring and X-ray and neutron imaging) have been evaluated as potential tools that can be used to detect the damage (cracking) caused by ASR. Passive acoustic emission monitoring has the potential to be used to determine the reactivity of the aggregate faster than current length change measurements. In addition, X-ray and neutron imaging are discussed as potential methods to detect cracking as well as to assess the impacts of cracks on transport properties of the matrix.

Passive Acoustic Emission Monitoring

Acoustic emission was investigated as an experimental technique that may be used to detect cracking due to ASR faster than current length change measurements. Figure 9 shows the length change of mortars made with reactive and non-reactive aggregates, and figure 10 shows the acoustic emission activity. A greater acoustic activity was observed in samples with reactive aggregate (TX1) as compared with samples with nonreactive aggregates (Ottawa).

Figure 9. Length change of ASTM mortar bars in 1 N NaOH solution during testing period.

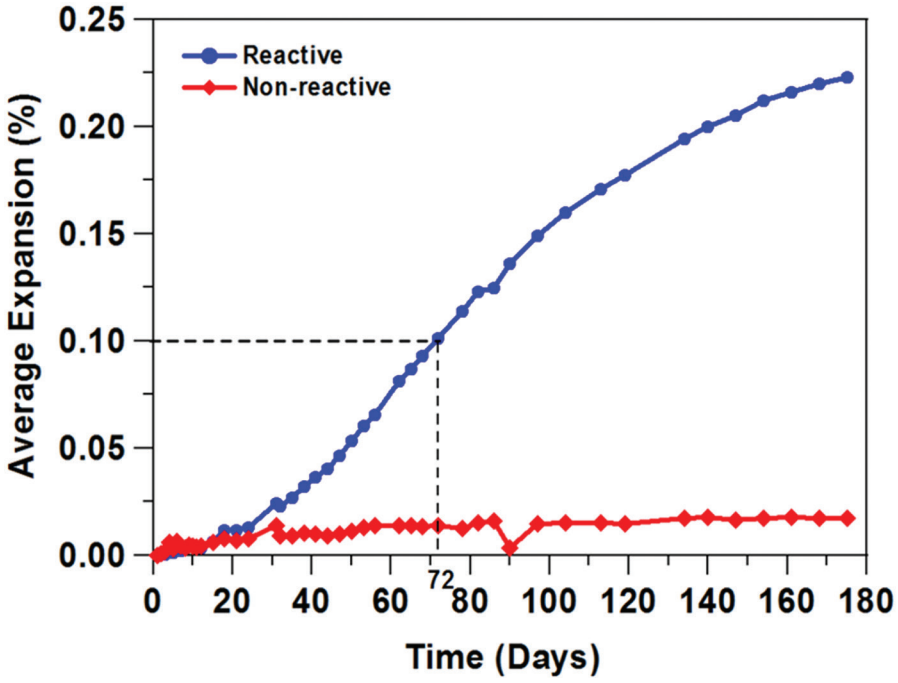

Figure 10. Cumulative acoustic emission energy for large mortar samples immersed in 1 N NaOH solution during testing period.

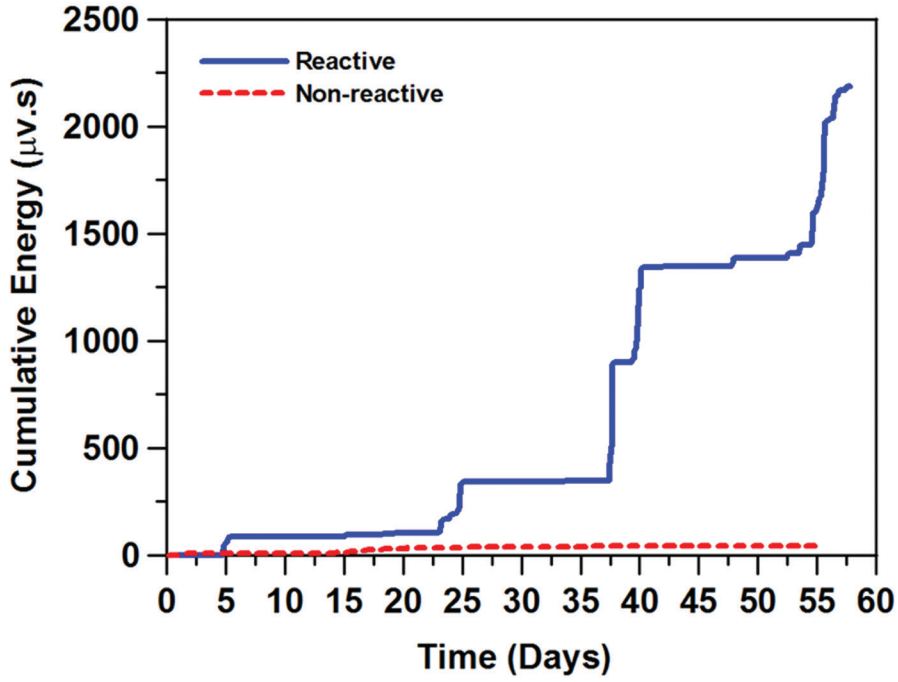

Acoustic activity was detected more easily at an earlier testing time, making the use of acoustic emission a potentially good approach for quantifying the onset of ASR cracking. Much more substantial reaction and cracking (resulting in longer testing times) is needed to assess the potential for ASR. The acoustic waves generated by cracking appear to show a frequency shift that correlates with a shift in cracking from the aggregate (onset of damage) to cracking in the matrix (at later ages).

X-ray and Neutron Imaging

X-ray and neutron radiography were used to investigate unsaturated fluid transport in cement-based materials (figure 11 and figure 12). Beer's Law was used to quantify fluid absorption, and the influence of solution properties (viscosity and surface tension) was captured both experimentally and numerically.[4] X-ray tomography shows promise; however, it does not appear to be able to capture the earliest cracking using the sample sizes tested in this work because of limits on resolution.

Implementation of Research Study Findings

The results and findings of this research suggest several potential approaches to determine the reactivity of aggregate, mitigate ASR, and detect the damage induced by ASR. These approaches include the following: 1) the advanced quick chemical test (AQCT), 2) use of the model to predict the minimum dosage of $LiNO_3$, 3) use of acoustic emission, and 4) X-ray and neutron imaging to detect damage caused by ASR.

AQCT

The proposed AQCT was developed using the thermodynamic modeling approach presented in the previous section. The methodology of the aggregate reactivity classification used in the AQCT is essentially the same as that used in the ASTM C289, the Standard Test Method for Potential Alkali-Silica Reactivity of Aggregates, also called the quick chemical test. However, the one distinct difference between those two methodologies is that the AQCT method replaces the laboratory testing required in the ASTM C289

Figure 11. X-ray tomography of samples—initial imaging.

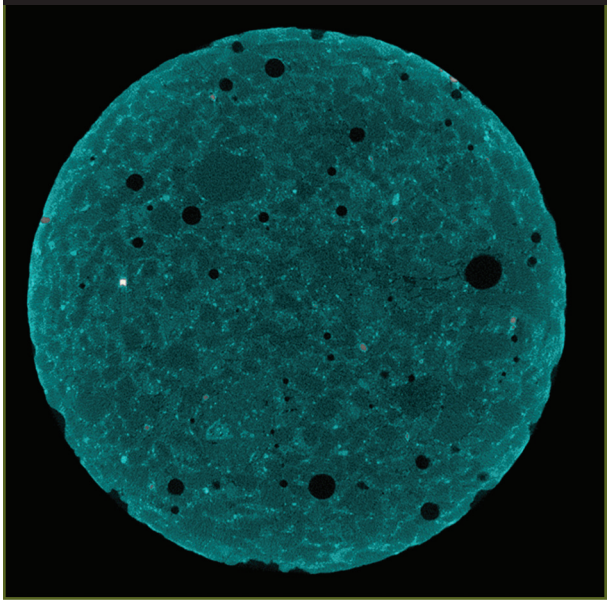

Figure 12. X-ray tomography of samples after 116 days of exposure to NaOH illustrating cracking due to ASR.

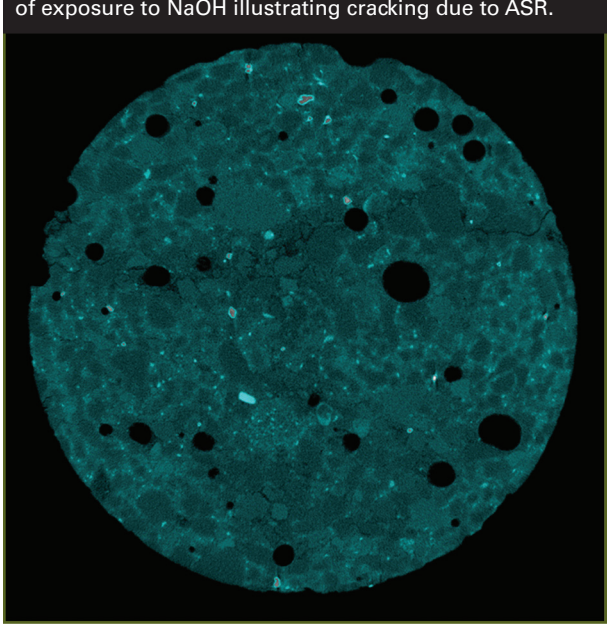

method with thermodynamic simulation, which utilizes the data on mineralogical composition of the aggregate as input value for the model.

The results obtained from the thermodynamic simulation are compared with the empirically derived criteria, which evaluate the reactivity of aggregates. Therefore, this approach is referred to as "semi-fundamental method to evaluate the reactivity of aggregates." AQCT can predict the reactivity of aggregates quite accurately. If further study was conducted to collect the required kinetic parameters for various types of silica minerals, then this test method can be modified or improved to increase the accuracy. In addition, because the AQCT method was developed based on the fundamental aspect of ASR—dissolution of silica and chemical steps involved in the ASR process—it represents a good example of how the fundamental study of ASR can lead to practical engineering solution.

Prediction of Minimum Dosage of $LiNO_3$

A developed model to predict the concentration of Li^+ ions in pore solution was implemented to determine the minimum [Li]/[Na+K] ratios required for various mixture designs from the value of minimum [Li]/[Na+K] obtained from just one particular design. The proposed method has potential for reducing number of trials needed to determine the minimum amount of $LiNO_3$ required for each of a different concrete mixture designs. Once the minimum dosage of $LiNO_3$ is determined for one concrete mixture design, the proposed method allows estimation of the minimum lithium-to-alkali molar ratio for a range of different mixture designs using the same reactive aggregate.

Implementation of Acoustic Emission

Acoustic emission is an experimental technique that is capable of determining the reactivity of the aggregate faster than current length change measurements. In samples containing reactive aggregates, substantially greater acoustic emission activity was observed than in samples with nonreactive aggregates. Samples with active ASR showed acoustic activity long before sufficient expansion occurred, suggesting the potential for using acoustic emission as an early detection technique and that the testing was more effective in larger samples, which would better facilitate concrete mixtures. The frequency of the acoustic wave shifts over time appears to correlate with a shift in cracking from the aggregate (onset of damage) to the cementitious matrix.

Implementation of X-ray and Neutron Imaging

X-ray and neutron imaging (radiography and tomography) are powerful tools for detecting cracking as well as the impact of cracks on fluid transport. While not immediately ready for use in quality control or acceptance testing, the use of X-ray or neutron imaging shows promise in aiding in the interpretation of experimental results or in the development of models that include the influence of cracking on the increased rate of ASR damage development. An approach was developed using Beer's Law to determine the moisture content; this is more promising for neutron imaging because of the higher sensitivity of the technique. While tomography technique is promising, its use for ASR damage detection is limited because of the restrictions on sample size and resolution. These restrictions make it difficult to detect the onset of damage. However, damage at later ages can be seen and used to supplement other measurements.

References

1. Stanton, T.E., "Expansion of concrete through reaction between cement and aggregate," *Proceedings of the American Society of Civil Engineers*, *66*, 1940, pp. 1,781–1,811.
2. Bérubé, M.A., C. Tremblay, B. Fournier, M.D. Thomas, and D.B. Stokes, "Influence of

lithium-based products proposed for counteracting ASR on the chemistry of pore solution and ccement hydrates," *Cement Concrete Research*, *34*(9), 2004, pp. 1,645–1,660.

3. Diamond, S., "Unique response of LiNO3 as an alkali silica reaction-preventive admixture," *Cement Concrete Research*, *29*(8), 1999, 1,271–1,275.

4. Pour-Ghaz, M., F. Rajabipour, J. Couch, and J. Weiss, "Modeling fluid transport in cementitious systems with crack-like (notch) geometries," International RILEM Workshop on Concrete Durability and Service Life Planning, 2009, Haifa, Israel.

Researcher—This study was performed by School of Civil Engineering, Purdue University, West Lafayette, Indiana, 47907, Contract No. DTFH61-08-R-00010.

Distribution—This TechBrief is being distributed according to a standard distribution. Direct distribution is being made to the Divisions and Resource Center.

Availability—The publication associated with this TechBrief is *Alkali-Silica Reaction Mecahnisms and Detection: An Advanced Understanding* (FHWA-HRT-14-078). It is available in print and online at http://www.fhwa.dot.gov/research.

Key Words—Alkali-silica reaction, thermodynamic model, reactive aggregates, lithium nitrate, deicers, passive acoustic emission, x-ray and neutron imaging.

OCTOBER 2014

FHWA-HRT-14-079
HRDI-60/10-14(600)